

Evaluation of the Imaging Properties of a CT Scanner with the Adaptive Statistical Iterative Reconstruction Algorithm

Noise, Contrast and Spatial Resolution Properties of CT Images Reconstructed at Different Blending Levels

Patrizio Barca^{1,3}, Marco Giannelli², Maria Evelina Fantacci^{1,3} and Davide Caramella⁴

¹Department of Physics, University of Pisa, Pisa, Italy

²Unit of Medical Physics, Pisa University Hospital “Azienda Ospedaliero-Universitaria Pisana”, Pisa, Italy

³INFN, Pisa Section, Pisa, Italy

⁴Department of Radiology, Pisa University Hospital “Azienda Ospedaliero-Universitaria Pisana”, Pisa, Italy

Keywords: CT Iterative Reconstruction, ASIR, Image Quality, NPS, CNR, MTF.

Abstract: X-ray Computed Tomography (CT) is an essential imaging technique for different diagnostic and therapeutic tasks. However, ionizing radiation from CT scanners represents the largest source of medical exposure for the population of industrialized countries. In order to reduce CT dose during patient examination, iterative reconstruction algorithms have been developed to help existing dose reduction methods. In this paper, we studied the image quality performance of a 64-slice CT scanner (Optima CT660, GE Healthcare, Waukesha, WI, USA) that implements both the conventional filtered back-projection (FBP) and the Adaptive Statistical Iterative Reconstruction (ASIR, GE Healthcare, Waukesha, WI, USA) algorithm. In order to compare the performance of these two reconstruction technologies, CT images of the Catphan®504 phantom were reconstructed using both conventional FBP and ASIR with different percentages of reconstruction from 20% to 100%. Noise level, noise power spectrum (NPS), contrast-to-noise ratio (CNR) and modulation transfer function (MTF) were estimated for different values of the main radiation exposure parameters (i.e. mAs, kVp, pitch and slice thickness) and contrast objects. We found that, as compared to conventional FBP, noise/CNR decreases/increases non-linearly up to 50%/100% when increasing the ASIR blending level of reconstruction. Furthermore, ASIR modifies the NPS curve shape (i.e. the noise texture). The MTF for ASIR-reconstructed images depended on both tube load and contrast level, whereas MTF of FBP-reconstructed images did not. For lower tube load and contrast level, ASIR offered lower performance as compared to conventional FBP in terms of reduced spatial resolution and MTF decreased with increasing ASIR blending level of reconstruction.

1 INTRODUCTION

In the last years, concerns about ionizing radiations exposure due to computed tomography (CT) technology have lead to develop strategies to optimize CT procedures (tube current modulation, automatic exposure control, advances in detection technology etc.) (McNitt-Gray, 2002). A promising approach for dose reduction is represented by the improvement of image reconstruction algorithms, that, in contrast with FBP algorithm, take into account a model of the imaging system to describe the different physical aspects of image acquisitions. This may offer the opportunity to reduce image

noise with respect to FBP reconstructions. Because of the strict correlation between radiation exposure and image noise, IR algorithms can be employed when CT data at reduced tube load product and/or tube potential (i.e. at reduced radiation exposure) are acquired (Willemink et al., 2013; Beister et al., 2012). Therefore, IR algorithms can be used with reduced radiation exposure without significantly affecting the diagnostic image quality with respect to conventional FBP (Willemink et al., 2013; Beister et al., 2012).

In this study, our attention was focused on a 64-slice CT scanner (Optima CT660, GE Helathcare, Waukesha, WI, USA) which implements both the conventional FBP algorithm and the Adaptive Statis-

tical Iterative Reconstruction (ASIR, GE Healthcare, Waukesha, WI, USA) algorithm (Willemink et al., 2013; Beister et al., 2012; Argaud, 2009).

ASIR works on raw data space modelling the fluctuations in the projection measurement and the noise characteristics of the scanned object (Argaud, 2009). Furthermore, ASIR offers the possibility of blending with FBP at various levels, from 0% (conventional FBP) to 100% ("pure" IR).

Previous works have shown that the noise reduction in the ASIR-reconstructed images is accompanied by changes in the noise texture as compared to FBP reconstruction, and the spatial resolution can vary as a function of dose and contrast (Richard et al., 2012; Samei et al., 2015; Miéville et al., 2013).

In our study, we quantitatively assessed noise level, noise power spectrum (NPS), contrast-to-noise ratio (CNR) and modulation transfer function (MTF) using different ASIR blending levels of reconstruction and a wide range of the main radiation exposure parameters (i.e. tube load, tube potential, pitch, slice thickness) values as well as different contrast objects.

The paper is organised as follows: after this brief introduction, we describe the materials and methods in which we present the image acquisition protocols and the adopted methodology for data analysis; in the next section, we describe the results in terms of the main image quality parameters analysed (noise level, NPS, CNR and MTF); then, we dedicate a section to the discussion of our results and finally we suggest our conclusions.

2 MATERIALS AND METHODS

2.1 Scanner and Phantom Acquisition

Images of the Catphan® 504 phantom (The Phantom Laboratory, NY, USA) were acquired with a 64-slice CT scanner (Optima CT660, GE Healthcare Waukesha, WI, USA). This phantom is composed of 4 modules with cylindrical shape (internal diameter of 15 cm). We employed the CTP486 module (a homogeneous water-equivalent module) and the CTP404 module (composed of many inserts of different materials in a water-equivalent background - nominal CT Hounsfield's units (HU) of the inserts are reported in the Catphan® 504 Manual).

For noise analysis, images of the CTP486 module were acquired varying the main acquisition parameters on a range of values as reported in Table 1. For spatial resolution evaluation, the CTP404

module was scanned across a range of acquisition parameters as reported in Table 2. The contrast-to-noise ratio (CNR) was computed from a subset of the images used in spatial resolution analysis. All images were reconstructed by using both conventional FBP and ASIR with different blending levels of reconstruction (20%, 40%, 60%, 80%, 100%).

2.2 Data Analysis

Image data analysis was performed using ImageJ (Wayne Rasband, National Institute of Health, USA) and OriginPro 9.0 (OriginLab Corporation, MA, USA) software packages.

2.2.1 Noise

Noise properties of ASIR reconstructed images were evaluated by measuring the standard deviation (SD) of HU values on a circular region of interest (ROI) (4.5 cm diameter) centered in the images. In addition, the noise power spectrum (NPS) was calculated from images acquired using a subset of the exposure parameters in Table 1 (tube load 112 mAs, tube potential 120 kVp, slice thickness 2.5 mm, pitch 0.984). We computed the 3D NPS (Siewerdsen et al., 2002; Verdun et al., 2015; Friedman et al., 2013) considering an ensemble of 20 volumes of interest (VOIs) selected from 19 slices. From each VOI we calculated the 3D NPS and then we made the ensemble average. In order to obtain a radial representation of NPS the $f_z=0$ plane of the 3D NPS was selected and a radial average was performed (Friedman et al., 2013).

2.2.2 Spatial Resolution

Spatial resolution properties of ASIR reconstructed images were assessed through the calculation of the modulation transfer function (MTF).

The MTF analysis was performed at different radiation exposure and considering 6 different inserts (air, PMP, LDPE, polystyrene, delrin and teflon). We adopted the circular edge method (Richard et al., 2012; Samei et al., 2015; Friedman et al., 2013; Takenaga et al., 2015) to compute the MTF. We acquired an ensemble 7 distinct images with the same scanning parameters and the MTF curves corresponding to the same insert were averaged. The uncertainty of the MTF estimation was obtained as the standard deviation of the above 7 measurements.

2.2.3 CNR

The CNR was obtained from 7 repeated acquisitions, using a subset of the acquisition parameters reported in Table 2 (tube load 140 mAs, 84 mAs, 56 mAs and 28 mAs). In this analysis, we considered polystyrene (low contrast), LDPE (medium contrast) and teflon (high contrast) inserts. The CNR was estimated as follows:

$$\text{CNR} = (\text{HU}_{\text{object}} - \text{HU}_{\text{bkg}}) / \sqrt{(\sigma_{\text{object}}^2 + \sigma_{\text{bkg}}^2)} \quad (1)$$

where $\text{HU}_{\text{object}}/\sigma_{\text{object}}$ and $\text{HU}_{\text{bkg}}/\sigma_{\text{bkg}}$ are the mean/standard deviation of HU values in a circle ROI in the insert and background region, respectively. For each insert, the CNR values were calculated from the mean value and its standard deviation (uncertainty) across the repeated acquisitions.

Table 1: Acquisition protocol/parameters for noise analysis.

Acquisition mode:	helical
Tube load (mAs):	28, 42, 56, 70, 84, 98, 112
Tube potential (KV):	80, 100, 120, 140
Tube rotation time (s):	0.7
Slice thickness (mm):	0.625, 1.25, 2.5, 3.75, 5, 7.5
Collimation along longitudinal direction (mm):	40
Pitch:	0.516, 0.984, 1.375
Number of reconstructed slices	19

Table 2: Acquisition protocol/parameters for spatial resolution and CNR analysis.

Acquisition mode:	helical
Tube load (mAs):	28, 56, 84, 112, 140, 168, 196, 224
Tube potential (KV):	120
Tube rotation time (s):	0.7
Slice thickness (mm):	2.5
Collimation along longitudinal direction (mm):	40
Pitch:	0.984
Number of reconstructed slices	19

3 RESULTS

3.1 Noise

Figure 1 shows noise with varying tube load, tube potential, slice thickness and pitch for conventional FBP algorithm and ASIR with different blending levels of reconstruction (20%, 40%, 60%, 80%, 100%). Noise decreased non-linearly with the increase of ASIR blending level of reconstruction as well as with increasing tube potential/tube load/slice thickness. On the other hand, noise increased with the increase of pitch value.

NPS results are reported in figures 2 and 3. ASIR algorithm acts as a low pass filter whose effect increases with the increase of blending level of reconstruction (Fig. 3).

3.2 Spatial Resolution

The spatial resolution results are reported in Figures 4 and 5. MTF of ASIR-reconstructed CT images varied with the contrast level (Fig. 4), especially at lower tube load. In particular, MTF decreased with decreasing contrast level. We also verified that MTF of FBP-reconstructed CT images was substantially independent of the contrast level and tube load. Furthermore, for ASIR-reconstructed CT images and lower contrast level, MTF decreased with decreasing tube load (Fig. 5 A). While for high contrast objects or high mAs values ASIR preserves the spatial resolution offered by FBP reconstruction , for lower tube load and contrast level, MTF of ASIR-reconstructed CT images was lower than MTF of conventional FBP-reconstructed images, and the first decreased with increasing blending level of reconstruction (Fig. 5 B).

3.3 CNR

CNR results are reported in Table 3. CNR values increased with increasing tube load. Also, for each tube load value and insert (teflon, LDPE, polystyrene), CNR values of ASIR-reconstructed CT images were higher than CNR values of conventional FBP-reconstructed CT images and increased non-linearly with increasing blending level of reconstruction.

Table 3: CNR values (mean \pm standard deviation) of teflon (high contrast)/ LDPE (medium contrast)/polystyrene (low contrast) inserts of the Catphan-CTP404 module for FBP- and ASIR-reconstructed CT images with different blending levels (20%, 40%, 60%, 80%, 100%). Tube load ranges from 140 mAs to 28 mAs and acquisition parameters are reported in Table 2.

	Teflon	LDPE	Polystyrene
<i>140 mAs</i>			
FBP	59.7 \pm 3.9	14.8 \pm 0.4	10.0 \pm 0.6
ASIR 20%	65.8 \pm 4.8	16.6 \pm 0.4	11.2 \pm 0.6
ASIR 40%	72.9 \pm 5.8	18.8 \pm 0.5	12.7 \pm 0.8
ASIR 60%	81.1 \pm 7.2	21.6 \pm 0.7	14.6 \pm 1.0
ASIR 80%	90.6 \pm 9.0	24.9 \pm 1.1	16.8 \pm 1.2
ASIR 100%	100.5 \pm 11.0	28.6 \pm 1.6	19.2 \pm 1.5
<i>84 mAs</i>			
FBP	41.4 \pm 3.6	11.1 \pm 0.3	7.4 \pm 0.5
ASIR 20%	52.7 \pm 4.1	13.1 \pm 0.4	8.8 \pm 0.6
ASIR 40%	58.6 \pm 5.7	14.8 \pm 0.4	10.0 \pm 0.7
ASIR 60%	65.5 \pm 7.0	16.9 \pm 0.8	11.5 \pm 1.0
ASIR 80%	73.6 \pm 8.8	19.4 \pm 1.0	13.3 \pm 1.3
ASIR 100%	82.5 \pm 10.2	22.2 \pm 1.5	15.4 \pm 1.4

	Teflon	LDPE	Polystyrene
<i>56 mAs</i>			
FBP	36.4 \pm 3.1	9.8 \pm 0.3	6.1 \pm 0.4
ASIR 20%	43.6 \pm 4.4	11.1 \pm 0.3	7.1 \pm 0.6
ASIR 40%	48.5 \pm 5.2	12.6 \pm 0.4	8.0 \pm 0.7
ASIR 60%	54.4 \pm 6.9	14.4 \pm 0.5	9.1 \pm 0.9
ASIR 80%	61.2 \pm 8.4	16.5 \pm 0.9	10.5 \pm 1.0
ASIR 100%	68.8 \pm 9.8	19.0 \pm 1.4	12.0 \pm 1.3
<i>28 mAs</i>			
FBP	26.8 \pm 2.8	6.8 \pm 0.3	3.4 \pm 0.3
ASIR 20%	31.2 \pm 3.0	3.3 \pm 0.3	4.9 \pm 0.4
ASIR 40%	35.1 \pm 4.3	8.3 \pm 0.3	5.5 \pm 0.4
ASIR 60%	39.8 \pm 6.3	9.5 \pm 0.5	6.3 \pm 0.6
ASIR 80%	45.5 \pm 7.0	10.9 \pm 0.7	7.3 \pm 0.8
ASIR 100%	51.9 \pm 7.4	12.6 \pm 0.7	8.4 \pm 1.0

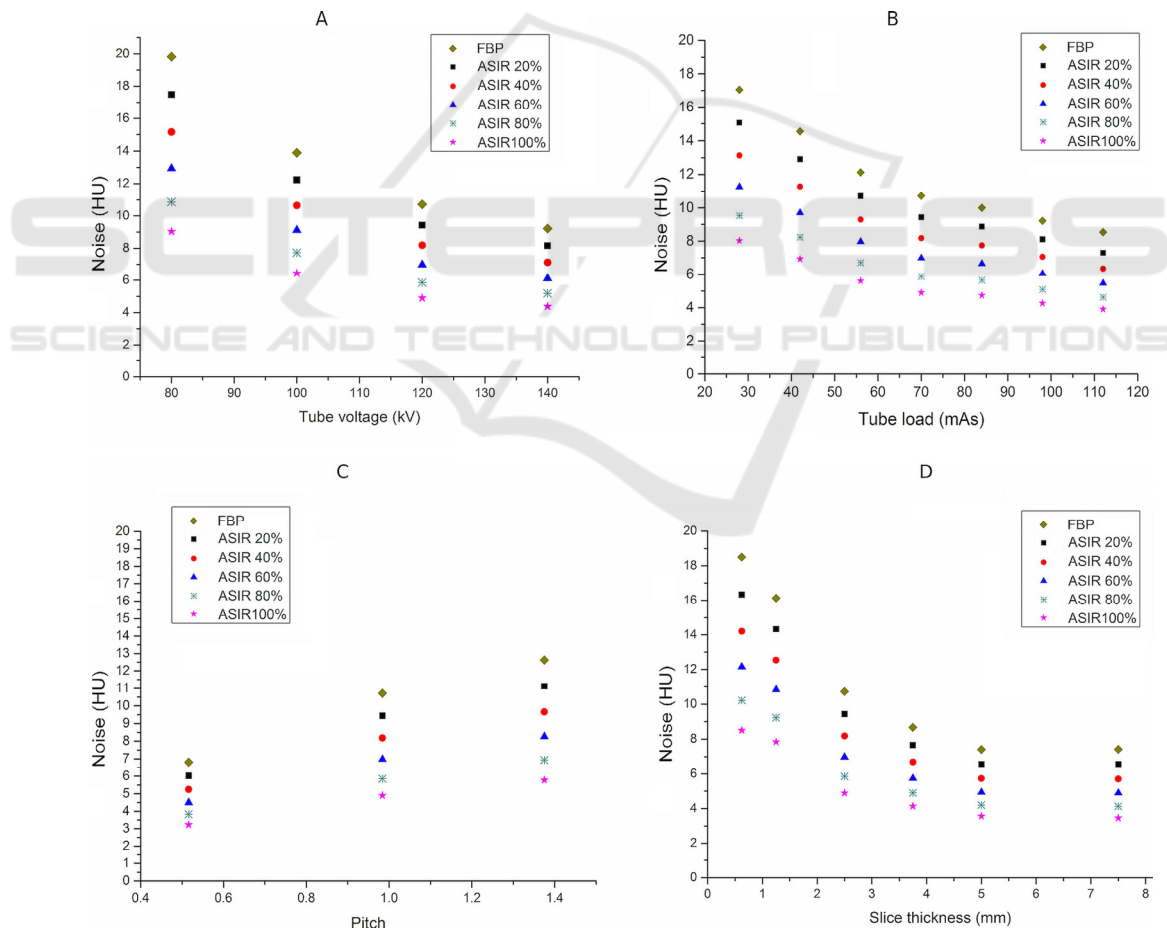


Figure 1: Noise (standard deviation) for conventional FBP algorithm and different ASIR blending levels of reconstruction (20%, 40%, 60%, 80%, 100%) with varying tube potential (tube load 112 mAs, pitch 0.984, slice thickness 2.5 mm) (panel A), tube load (tube potential 120 kVp, pitch 0.984, slice thickness 2.5 mm) (panel B), pitch (tube potential 120 kVp, tube load 112 mAs, slice thickness 2.5 mm) (panel C) and slice thickness (tube potential 120 kVp, tube load 112 mAs, pitch 0.984) (panel D).

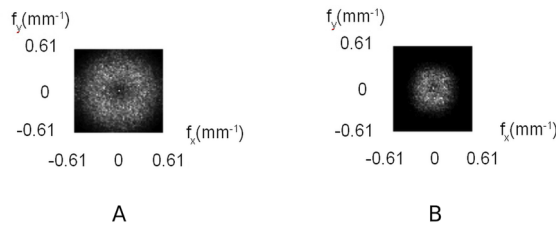


Figure 2: Visualization of the 3D NPS with respect to the plane $f_z = 0$ for conventional FBP (A) and ASIR with a blending level of reconstruction of 100% (B). (The maximum spatial frequency was determined by applying the Nyquist sampling criterion). Images were acquired at 120 kVp, 112 mAs, slice thickness 2.5 and pitch 0.984.

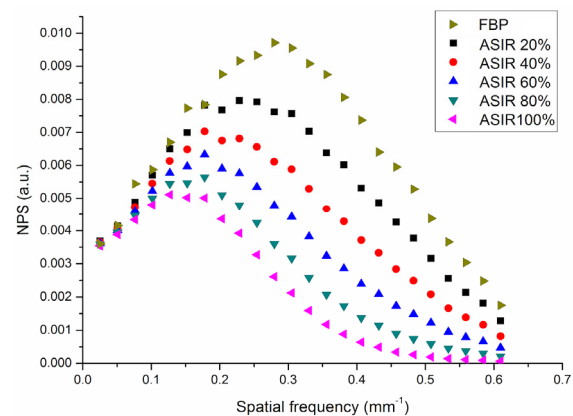


Figure 3: Example (same parameters as Fig. 2) of radial NPS for conventional FBP algorithm and ASIR algorithm with different blending levels of reconstruction.

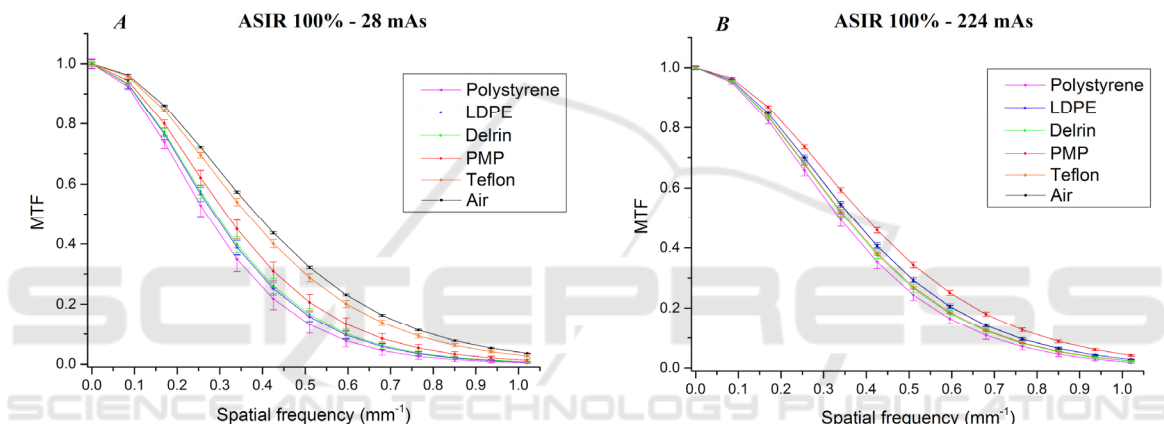


Figure 4: MTF for ASIR-reconstructed CT images (blending level of reconstruction of 100%) and low (28 mAs) (panel A)/high (224 mAs) (panel B) tube load, with varying contrast level (polystyrene, LDPE, delrin, PMP, teflon, air). Acquisition parameters are reported in Table 2.

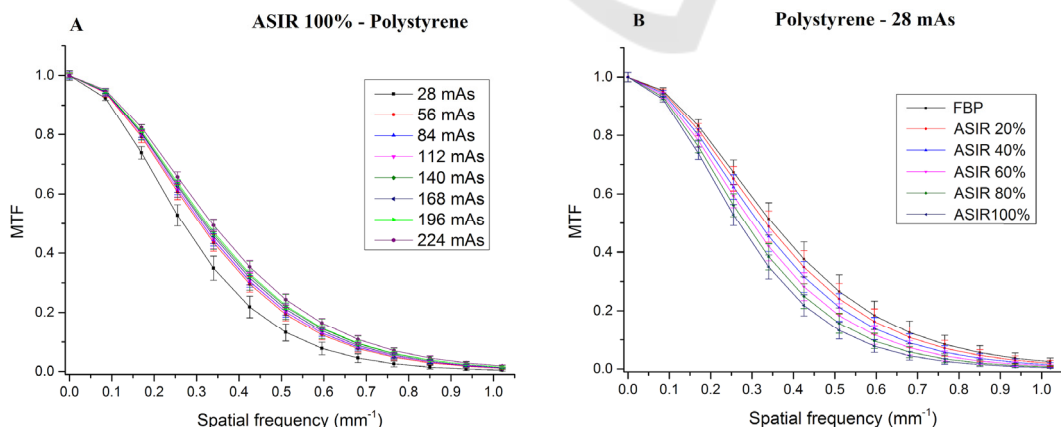


Figure 5: MTF for ASIR-reconstructed CT images (blending level of 100%) and low (polystyrene) contrast level, with varying tube load (28 mAs, 56 mAs, 84 mAs, 112 mAs, 140 mAs, 168 mAs, 196 mAs, 224 mAs), (panel A). MTF for low (28 mAs) tube load and low (polystyrene) contrast CT images, with varying reconstruction methods (FBP (black), ASIR with 20% (red), 40% (blue), 60% (magenta), 80% (green) and 100% (cyan) of blending level of reconstruction), (panel B). Acquisition parameters are reported in Table 2.

4 DISCUSSION

In this quantitative phantom study, CT image quality performance of two different reconstruction technologies have been carefully evaluated.

We comprehensively characterised the physical properties (in terms of several quality parameters such as noise, NPS, MTF and CNR) of the ASIR-reconstructed CT images using different blending levels of reconstruction in a number of experimental designs.

Our findings confirm the dose reduction potential of ASIR (Richard et al., 2012; Samei et al., 2015; Miéville et al., 2013; Smith, 2014 et al.; Brady et al., 2012; McCollough et al., 2015; Yanagawa et al., 2010). As compared to conventional FBP, noise/CNR decreases (Fig. 1)/increases (Table 3) up to 50%/100% when using ASIR. Also, ASIR does not modify the typical noise dependence on the acquisition parameters. Furthermore, the noise and CNR vary non-linearly with the ASIR blending level of reconstruction. In addition, NPS analysis (Fig. 3) shows that ASIR acts as a low-pass filter and modifies noise texture: for ASIR-reconstructed CT images, the frequency of the maximum of the NPS curve shifts non-linearly toward lower frequencies with increasing blending level of reconstruction, in agreement with the results of previous studies (Samei et al., 2015; Miéville et al., 2013).

We assessed the spatial resolution by estimating the MTF at different contrasts and exposure values. We found that, unlike conventional FBP, the MTF decreases with decreasing contrast and tube load. It should be noted that, for lower contrast and tube load, the MTF of ASIR-reconstructed images is lower than that of FBP-reconstructed images, and decreases with increasing blending level of reconstruction.

Recent studies have shown that these effects may affect low-contrast resolution and thus may influence the performance of automatic contour detection software (Precht et al., 2016).

When compared to conventional FBP reconstruction, ASIR allows for an improvement of image quality in terms of reduced noise and increased CNR, and hence a potential dose reduction in CT imaging can be obtained while preserving diagnostic capabilities. However, ASIR can modify noise texture as well as affect spatial resolution at low contrast and radiation exposure. For these reasons, the optimal ASIR blending level of reconstruction (i.e. the best trade-off between image quality and dose reduction) should be assessed for each specific

application through quantitative as well as subjective analysis.

Because of the noise reduction and CNR increment offered by ASIR, CT examinations can be performed at reduced radiation exposure levels. However, in order to avoid potential effects of losses in spatial resolution, which are inherent to ASIR and may reduce the diagnostic value of CT images, the optimal blending level of reconstruction should be assessed for each specific clinical application.

In this regard, CT follow-up examinations (Lim et al., 2016; Precht et al., 2016) and screening programs could benefit of this new reconstruction technology. In particular, the use of ASIR in CT screening programs – aimed at detecting small contrast lesions with low dose – should be carefully evaluated.

5 CONCLUSIONS

A relevant noise reduction and CNR increment in CT images are achieved with the ASIR algorithm with respect to the conventional FBP reconstruction in different experimental designs. For this reason, the iterative reconstruction approach represents an effective method for optimizing dose in CT imaging. However, for low dose and low contrast acquisitions (typical for instance of screening programs) ASIR can provide lower performance, in terms of reduced spatial resolution capabilities, as compared to conventional FBP, and its use, along with the choice of the optimal blending level of reconstruction, should therefore be carefully evaluated.

Moreover, this work lays the basis for further studies on CT imaging with ASIR. In particular, our recent interests are focused on the performance of a Computed Aided Detection (CAD) system with ASIR-reconstructed clinical images of the lung. In fact, the CAD system has been developed by taking into account the FBP-related appearance of the images and therefore, an investigation on the CAD response to the ASIR-reconstructed images could be of considerable interest.

ACKNOWLEDGEMENTS

We would like to thank Prof. Duccio Volterrani, Prof. Antonio Claudio Traino and Dr. Davide Giustini for supporting this work.

REFERENCES

- McNitt-Gray M. F., 2002. AAPM/RSNA Physics tutorial for residents: Topics in CT. Radiation dose in CT. *Radiographics*; 22(6):1541–53.
- Willemink M. J., de Jong P. A., Leiner T., de Heer L. M., Nieuvelstein RA, Budde R. P., Schilham AM., 2013. Iterative reconstruction techniques for computed tomography Part 1: Technical principles. *European Radiology*; 23:1623–31.
- Beister M., Kolditz D., Kalender W. A., 2012. Iterative reconstruction methods in X-ray CT. *Physica Medica*; 28(2):94-108.
- Argaud C. ASIR: a new reconstruction technique to lower dose without compromise, *ASIR whitepaper*. GE Healthcare (Waukesha, WI, USA).
- Richard S., Husarik D. B., Yadava G., Murphy S. N., Samei E., 2012. Towards task-based assessment of CT performance: system and object MTF across different reconstruction algorithms. *Medical Physics*; 39(7): 4115-22.
- Samei E. and Richard S. Assessment of the dose reduction potential of a model-based iterative reconstruction algorithm using a task-based performance metrology. *Medical Physics* 2015; 42(1):314-23.
- Miéville F. A., Gudinchet F., Brunelle F., Bochud F. O., Verdun F. R., 2013. Iterative reconstruction methods in two different MDCT scanners: Physical metrics and 4-alternative forced-choice detectability experiments – A phantom approach. *Physica Medica*; 2:99-110.
- Siewerdsen J. H., Cunningham I. A., Jaffray D. A., 2002. A framework for noise-power spectrum analysis of multidimensional images. *Medical Physics*; 29(11):2655-71.
- Verdun F. R., Racine D., Ott J. G., Tapiovaara M. J., Toroi P., Bochud F. O., Veldkamp W. J., Schegerer A., Bouwman R. W., Giron I. H., Marshall N. W., Edyvean S., 2015. Image quality in CT: From physical measurements to model observers. *Physica Medica*; 31(8):823-43.
- Friedman S. N., Fung G. S. K., Siewerdsen J. H., Tsui B. M. W., 2013. A simple approach to measure computed tomography (CT) modulation transfer function (MTF) and noise-power spectrum (NPS) using the American College of Radiology (ACR) accreditation phantom. *Medical Physics*; 40(5):051907.
- Takenaga T., Katsuragawa S., Goto M., Hatemura M., Uchiyama Y., Shiraishi J., 2015. Modulation transfer function measurement of CT images by use of a circular edge method with a logistic curve-fitting technique. *Radiological Physics and Technology*; 8:53–59.
- Smith E. A., Dillman J. R., Goodsitt M. M., Christodoulou E. G., Keshavarzi N., Strouse P. J., 2014. Model-based iterative reconstruction: Effect on patient radiation dose and image quality in pediatric body CT. *Radiology*; 270(2):526-34.
- Brady S. L., Yee B. S., Kaufman R. A., 2012. Characterization of adaptive statistical iterative reconstruction algorithm for dose reduction in CT: A pediatric oncology perspective. *Medical Physics*; 39(9):5520-31.
- McCollough C. H., Yu L., Kofler J. M., Leng S., Zhang Y., Li Z., Carter R. E., 2015. Degradation of CT low-contrast spatial resolution due to the use of iterative reconstruction and reduced dose levels. *Radiology*; 276(2):499-506.
- Yanagawa M., Honda O., Yoshida S., Kikuyama A., Inoue A., Sumikawa H., Koyama M., Tomiyama N., 2010. Adaptive statistical iterative reconstruction technique for pulmonary CT: image quality of the cadaveric lung on standard- and reduced-dose CT. *Academic Radiology*; 17(10):1259-66.
- Lim H., Chung M. J., Shin K. E., Hwang H. S., Lee K. S., 2016. The impact of Iterative Reconstruction in Low-Dose Computed Tomography on the Evaluation of Diffuse Interstitial Lung Disease. *Korean Journal of Radiology*; 17(6):950-60.
- Precht H., Kitslaar P. H., Broersen A., Dijkstra J., Gerke O., Thygesen J., Egstrup K., Lambrechtse J., 2016. Influence of Adaptive Statistical Iterative Reconstruction on coronary plaque analysis in coronary computed tomography angiography. *Journal of Cardiovascular Computed Tomography*; 10(6):507-16.

SPRINGER
SCIENCE AND TECHNOLOGY PUBLICATIONS